AIAA JOURNAL
Vol. 30, No. 3, March 1992

Finite Element Navier-Stokes Solver for Unstructured Grids

D. L. Marcum* and R. K. Agarwal†
McDonnell Douglas Corporation, St. Louis, Missouri 63166

A three-dimensional finite element Navier-Stokes solver has been developed for calculating transonic viscous flow on unstructured grids about complex aerodynamic configurations. The solver employs a second-order-accurate space discretization of the Navier-Stokes equations obtained from a Galerkin weighted-residual approximation. Time discretization is obtained using either an explicit two-step Lax-Wendroff scheme, or an explicit multistep Runge-Kutta scheme. Boundary conditions are implemented using a procedure based on the method of characteristics. The overall solution procedure has been initially validated by calculating two- and three-dimensional inviscid and viscous transonic flows.

Introduction

ADVANCES in computer technology and numerical algorithms are making possible the use of computational fluid dynamics to analyze configurations with realistic and complex geometries. As configurations of greater complexity are analyzed, the task of generating a suitable grid for the analysis becomes increasingly difficult. More effort may be required to generate the grid for a complex configuration than to obtain the flowfield solution. In addition, grid generation is further complicated in some cases by the need to adapt the grid as the solution progresses to resolve complex flow features accurately. This is especially true for unsteady flowfields with moving components. Considerable effort has recently been devoted to research on unstructured grid technology as this approach can readily be used to subdivide domains of arbitrary complexity and is ideally suited to grid adaptation. This technology has the potential to reduce significantly the effort required to generate grids for complex configurations and to increase the quality of the solutions. Many of the techniques developed for structured grid flow solvers are not extendible or require significant modification for use with unstructured grids. Consequently, development work on both unstructured grid generators and flow solvers is required.

Several procedures for calculating three-dimensional inviscid flowfields using unstructured grids have been developed and successfully applied to complex configurations (Jameson et al.,[1,2] Löhner et al.,[3,4] Peraire et al.,[5] and Stoufflet et al.[6]). For calculating viscous flowfields, considerably less work has been published using unstructured grids. In two dimensions, procedures have been presented using algebraic turbulence models by Mavriplis,[7] Kallinderis and Baron,[8] and Rostand[9] and using a k-ε turbulence model by Holmes and Connell.[10] Nakahashi and Obayashi[11] have calculated two- and three-dimensional viscous flowfields using a fully structured scheme with an algebraic turbulence model in viscous flow regions and a connecting inviscid unstructured scheme. For three-dimensional laminar flow, Hassan et al.[12] have presented a scheme using a pseudo-unstructured grid in viscous flow regions and Bristeau et al.[13] have presented a scheme using a fully unstructured grid. The hybrid structured/unstructured grid approach offers considerable advantages for streamlined bodies with well-defined viscous regions. For more complex configurations or cases where the viscous regions are not well defined a priori, a fully unstructured scheme may be more advantageous. Based on the very successful inviscid flow results and the promising but limited results for viscous flow, there is a need for considerably more research into applying unstructured grid technology to viscous flowfields.

The primary objective of the present effort is to develop a working code for investigation of viscous flowfield calculations using unstructured grid technology. This paper describes the development of a three-dimensional finite element Reynolds-averaged Navier-Stokes solver that achieves this objective. The solver uses a second-order-accurate space discretization of the Navier-Stokes equations obtained from a Galerkin weighted-residual approximation. The solution domain is divided into an unstructured grid containing tetrahedral or triangular elements. Time discretization is obtained using either an explicit two-step Lax-Wendroff scheme or an explicit multistage Runge-Kutta scheme. Boundary conditions are implemented using a procedure based on the method of characteristics. A two-equation k-ε turbulence model is used.

Governing Equations

The governing equations employed in the present work are the Reynolds-averaged Navier-Stokes equations expressed in conservation form for time-dependent, three-dimensional, compressible flow of a simple system in thermodynamic equilibrium in the absence of body forces. The thermodynamic model used is that of a thermally and calorically perfect gas. Other thermodynamic models can be incorporated.

Turbulence Model

For most viscous flowfields about aircraft configurations, a laminar flow assumption is not valid. Consequently, a turbulence model must be incorporated to account for the effects of turbulence. After careful consideration, it was determined that a field equation turbulence model is required to accurately compute flowfields about complex configurations or flowfields with detached viscous regions. Since the primary objective for the present work is to develop a code to compute flowfields such as these, a k-ε turbulence model was chosen for implementation. With a k-ε model the turbulent coefficients of viscosity and thermal conductivity are determined from the turbulence kinetic energy and dissipation rate which are obtained from coupled transport equations. Both the low-Reynolds-number and high-Reynolds-number models of Jones, Launder, and Spalding[14,15] are implemented in the present procedure. The k-ε transport equations are described in Refs. 14–16.

Presented as Paper 90-1652 at the AIAA 21st Fluid Dynamics, Plasma Dynamics, and Lasers Conference, Seattle, WA, June 18–20, 1990; received Oct. 15, 1990; revision received June 20, 1991; accepted for publication June 29, 1991.

*Scientist, McDonnell Douglas Research Laboratories. Member AIAA.

†Program Director, McDonnell Douglas Research Laboratories. Associate Fellow AIAA.

Numerical Solution Procedure

The governing equations and the k-ε equations are solved by either an explicit multistep Runge-Kutta scheme or an explicit two-step Lax-Wendroff scheme. The Runge-Kutta scheme is based on the procedures developed in Refs. 1 and 17, and the Lax-Wendroff scheme is based on the procedures developed in Refs. 5 and 18. A brief description of these schemes and the overall solution procedure is presented below. A complete description is presented in Ref. 16.

Finite Element Discretization

The conservation form of the governing equations are discretized in space using a Galerkin weighted-residual approximation with the solution domain divided into tetrahedral finite elements. The conservative variable solution unknowns are stored and solved for at the element nodes. In the Galerkin weighted-residual approximation, spacial discretization is obtained using piecewise linear test and shape interpolating functions. The resulting discretization is equivalent to that which can be obtained using a finite volume approach. For example, the inviscid flux terms are evaluated at each element face by taking the dot product of the face area vector and the average of the flux vector evaluated at the three element nodes on the face. At an element node, the inviscid flux residual contribution is the sum of the flux terms evaluated at each element face adjacent to the element node.

Discretization in time is obtained using either an explicit multistep Runge-Kutta scheme or on explicit two-step Lax-Wendroff scheme. In the present investigation, a four-step, fourth-order accurate in time Runge-Kutta scheme is used.

Artificial Diffusion

In regions containing severe gradients, e.g., near shock waves and stagnation points, artificial diffusion is required with both the Runge-Kutta and Lax-Wendroff schemes to filter out oscillations. The Runge-Kutta scheme also requires background artificial diffusion to filter out oscillations from decoupling. For the Lax-Wendroff scheme an adaptive second-order filter is used. And for the Runge-Kutta scheme the same filter is used, blended with a fourth-order background filter.

The second-order filter is evaluated at each element side by taking the product of a pressure gradient sensitive coefficient and the difference between the unknowns at the two element nodes on the side. At an element node, the resulting contribution is the sum of the filter terms evaluated at each element side attached to the element node. The pressure gradient-sensitive coefficient is obtained in a similar manner by summing the side differences of the pressure.

For the fourth-order filter, two applications of a second-order filter are used. First, the second-order differences are obtained by summing the side differences of the unknown. Then, the side differences of the second-order differences are summed to obtain the fourth-order filter contribution at an element node. Mach number scaling is used to reduce fourth-order filter contributions in boundary layers.

For enhanced resolution of severe gradients, a flux-corrected transport (FCT) algorithm[18-20] is an option available instead of the second-order filter. The present implementation follows that of Ref. 18, with one exception. The FCT limiting procedure is performed on element side contributions rather than on element contributions.

Boundary Conditions

The method of characteristics can be used to obtain characteristic compatibility equations which contain directional derivatives along the physical paths of propagation. References 21 to 23 present derivations of these compatibility equations. For the present work, the compatibility equations are obtained by choosing density, pressure, and velocity as dependent variables and characteristic surface vectors which are aligned with the boundary. To implement the boundary conditions, the characteristic compatibility equations could be integrated directly along their respective paths of propagation. It has been demonstrated[24,25] that this is a very accurate procedure, and that alternative schemes, such as Kentzer's method,[26] can yield comparable accuracy with superior efficiency. In Kentzer's method, the directional derivatives of the characteristic compatibility equations are expressed in partial derivative form and integrated at all boundary points by the same procedure used at interior points. In the present work, the original conservation form of the governing equations are integrated by the same procedure at all points in the computational domain and then a characteristic corrector procedure is applied at boundary points. This procedure can be derived using a linearized or one-dimensional form of the compatibility equations. It can also be derived from the complete characteristic compatibility equations by using the solution obtained without boundary condition correction to replace the source terms and spatial partial derivatives in those equations. The use of this procedure results in a method which is essentially equivalent to Kentzer's method with improved efficiency. The boundary conditions for far-field/near-field, subsonic/supersonic, inflow/outflow boundary points are implemented using this characteristic corrector procedure.

For a free-slip solid boundary point, the velocity normal to the boundary is set to zero. In addition, the mass, momentum, and energy flux can be set to zero at boundary faces containing free-slip boundary points as suggested by Mavriplis.[17]

At a no-slip solid boundary point, the velocity vector is set to zero, the pressure is extrapolated, and the temperature is set using either an isothermal or adiabatic boundary condition.

For turbulent flow, the turbulence dissipation rate and kinetic energy boundary conditions are set at all inflow/outflow boundaries using the previously described method of characteristics procedure.

At a no-slip solid boundary point, the turbulence dissipation rate and kinetic energy are set to zero for the low-Reynolds-number turbulence model.

With the low-Reynolds-number turbulence model, near-wall effects are accounted for with appropriate source terms and modeling coefficients. For the high-Reynolds-number model, near-wall effects must be accounted for with proper boundary conditions. For the high-Reynolds-number model, the turbulence dissipation rate and kinetic energy at points adjacent to a no-slip solid boundary are determined from relations dependent on the friction velocity and the normal distance between the boundary and the adjacent point. The friction velocity is obtained from a linear, blended, or logarithmic law of the wall. For turbulent flow calculations, the nodes adjacent to a no-slip solid boundary are chosen, when possible, to be located within the linear range with a y^+ less than five. No additional constraints on the flow variables are imposed at adjacent points, as is common practice with the high-Reynolds-number model. Without additional constraints, the velocity profile near the wall is computed, not assumed, and should provide a more accurate estimate of the skin friction.

The boundary conditions described in this section are applicable to structured as well as unstructured schemes. They have been successfully implemented in a structured grid flow solver and applied to a wide variety of configurations by Gielda et al.[27] For node-centered solvers the boundary condition procedures can be applied at the boundary nodes, as in the present work, and for element-centered solvers the boundary condition procedures can be applied at the boundary faces.

Computer Implementation

The numerical procedure described above has been implemented in a computer code named MDFENS. This code has been installed and executed on Convex C1, Cray X-MP, Cray-2, and Cray Y-MP computers. On each of these computers, the code is automatically vectorized without compiler directives wherever vectorization is possible. The code is com-

pletely vectorized with the exception of some setup and output sections which account for a small fraction of the total CPU time. To maintain portability, the code is written in "standard" Fortran. Memory and CPU requirements for MDFENS are listed in Table 1. Memory requirements can be adjusted approximately ±15% by varying the maximum vector length; those listed in Table 1 correspond to a maximum vector length of 10,000 words. When the FCT filter is used, the memory requirements increase by ~5% and the CPU requirements increase by ~20% with the Runge-Kutta scheme and ~40% with the Lax-Wendroff scheme.

Computed Examples

Several flowfields were computed to verify the accuracy of solutions obtained with the numerical procedure developed in this investigation. The results of these computations are presented below.

In all cases the initial flowfield properties were set to free-stream conditions and the steady-state solutions presented were obtained by marching in time until the residuals had been reduced by three or more orders of magnitude.

For most of the cases, the unstructured grid used was obtained from a structured grid as the geometries considered are simple. The intent here is not to demonstrate the ability to compute complex geometries using an unstructured grid, which has been done for inviscid flow by several researchers.[1-6] Rather, the intent is to validate initially the accuracy of the present procedure by analyzing inviscid and viscous cases with exact solutions or cases that are widely used for validation. For more complex configurations, there are primarily two methods that have been proposed for generating three-dimensional unstructured finite element type grids. One is based on Delaunay triangulation[28,29] and the other is based on the advancing-front method.[30,31] Currently, for complex configurations we use an advancing-front grid-generation code developed by Löhner.[31]

Subsonic Sink Flow

A planar, inviscid, subsonic sink flow was analyzed to verify the computed results against a known, exact solution. The three grids used contained 66, 231, and 861 nodes. The 231-node grid is illustrated in Fig. 1. The grid spacing for the 231-node grid is half that for the 66-node grid and the grid spacing for the 861-node grid is half that for the 231-node grid. The Mach number varies from 0.1 at the inlet upper wall to 0.8 at the exit lower wall. Figure 2 shows the effect of grid spacing on overall error using the Lax-Wendroff and Runge-Kutta schemes. The overall error in axial momentum is shown as it is the least accurately computed unknown for this case. The second-order accuracy of the calculations is evident by the slope of the curves in Fig. 2. The Lax-Wendroff and Runge-Kutta schemes produce comparable overall errors. Similar results have been obtained for supersonic source flow.[16]

Table 1 Memory and CPU requirements

	3-D Runge Kutta	3-D Lax-Wendroff			
	Inviscid	Inviscid	Laminar	Turbulent	
Memory (words/node)	130	140	140	150	
CPU time using one processor (μSEC/node-step)	165	64	–	–	Cray X-MP (MDC)
	167	65	–	–	Cray-2 (NASA-Ames)
	57	24	37	60	Cray Y-MP (NASA-Ames)

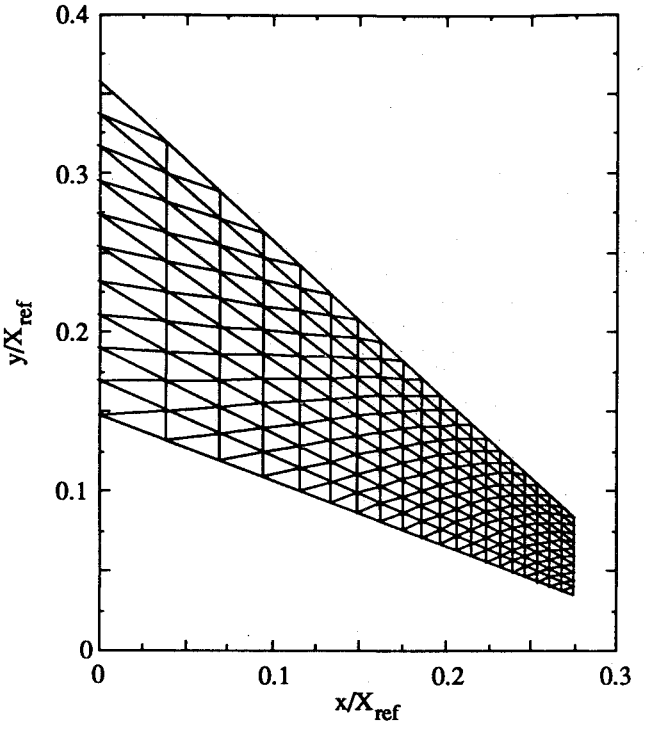

Fig. 1 Grid for subsonic sink flow with 400 elements and 231 nodes.

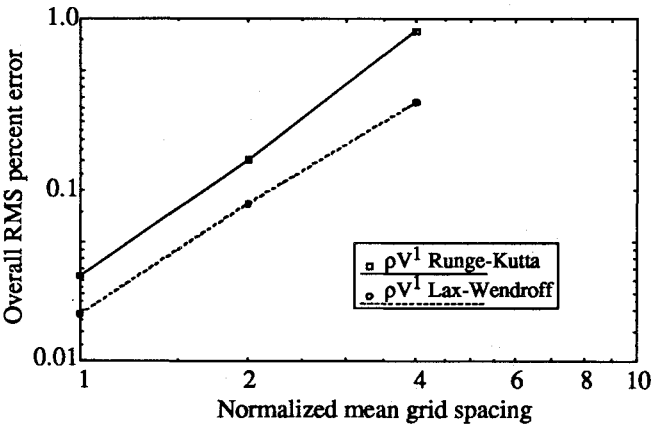

Fig. 2 Error convergence for subsonic sink flow.

NACA 0012 Airfoil

The inviscid flow about a NACA 0012 airfoil was analyzed to evaluate the results for a widely computed two-dimensional case. The case considered is that with a far-field Mach number of 0.8 and angle of attack of 1.25 deg. The 4966-node grid used is illustrated in Fig. 3. Pressure coefficient distributions on the airfoil surface are presented in Fig. 4 for computed solutions obtained using the Lax-Wendroff and Runge-Kutta schemes with the standard second-order filter and the FCT filter. All of the computed results are in good agreement with each other and with the results obtained by other researchers using structured and unstructured schemes. The FCT filter produces results with increased shock wave resolution, capturing both the upper and lower surface shock waves within

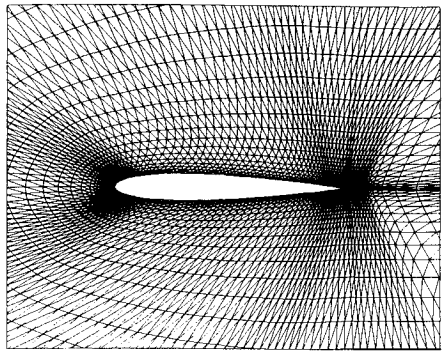

Fig. 3 Grid with 9600 elements and 4966 nodes for NACA 0012 airfoil.

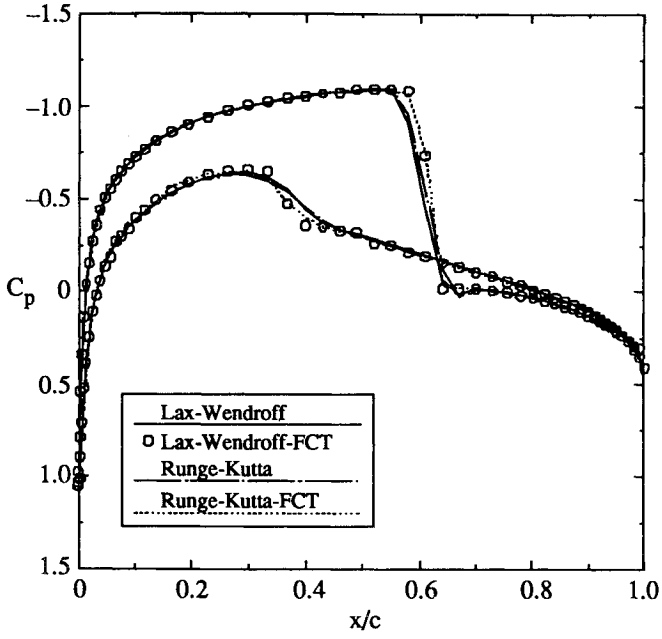

Fig. 4 C_p distributions for NACA 0012 airfoil at $M_\infty = 0.8$ and $\alpha = 1.25$ deg.

two elements. With the standard filter, shock waves are captured within three of four elements.

Laminar Flat Plate Flow

Laminar flow over a flat plate was analyzed to verify the accuracy of the computed results in a viscous flowfield. The two grids used contained 441 and 1681 nodes. The grid spacing for the 1681-node grid is half that for the 441-node grid in all directions. The 441-node grid is illustrated in Fig. 5. The far-field Mach number is 0.5.

Figure 6 shows the skin-friction coefficient distributions for the computed solutions obtained using the Lax-Wendroff and Runge-Kutta schemes, and the Blasius solution. The two computed solutions are in excellent agreement with the Blasius solution and with each other. The computed solutions for the two grids differ only near the leading edge, where the solution for the finer grid is more accurate.

Figure 7 shows the tangential velocity distributions for the computed solutions obtained using the Lax-Wendroff and Runge-Kutta schemes, and the Blasius solution. The two computed solutions are in very good agreement with the Blasius solution and with each other except at the edge of the boundary layer, where the Runge-Kutta solution is slightly degraded by the fourth-order background dissipation. The computed

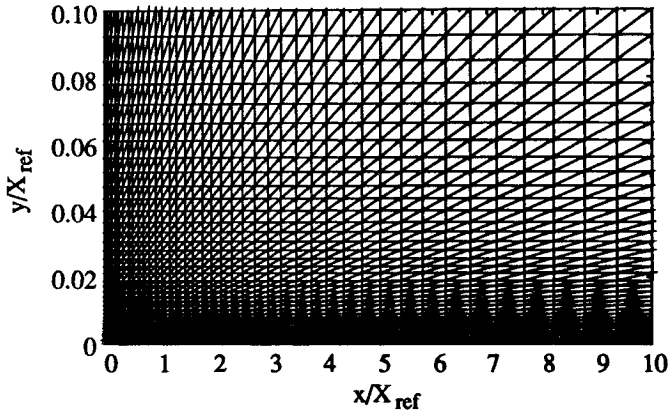

Fig. 5 Grid for laminar flat plate flow with 800 elements and 441 nodes.

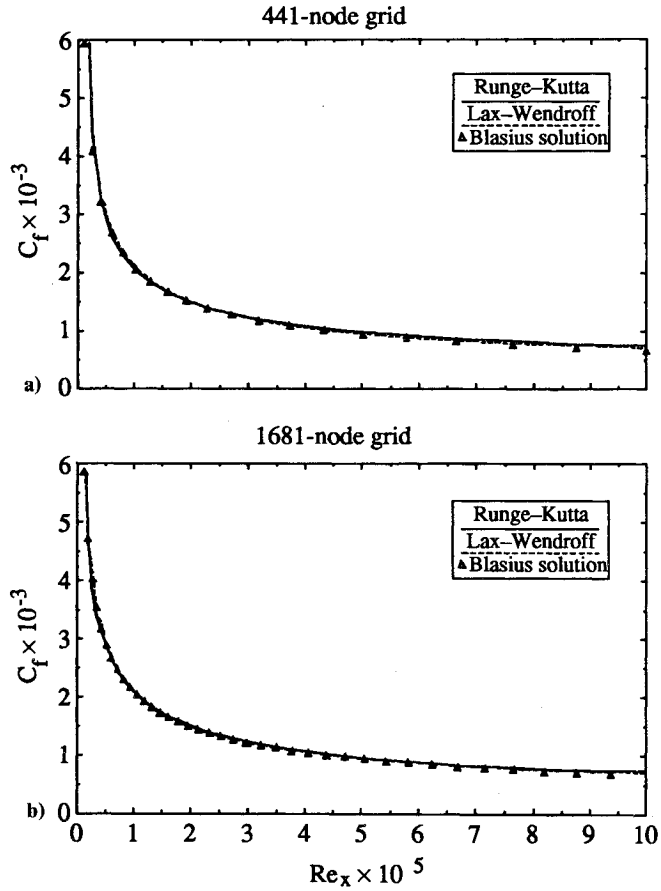

Fig. 6 C_f distributions for laminar flat plate flow at $M_\infty = 0.5$: a) for 441-node grid; b) for 1681-node grid.

solutions for the two grids differ only near the edge of the boundary layer, where the solution for the finer grid is more accurate. Also, the differences between the Runge-Kutta and Lax-Wendroff solutions are lessened with the finer grid.

The fourth-order dissipation used in the Runge-Kutta scheme is minimized by using a value for the overall dissipation coefficient which is just adequate for stability, and by scaling the coefficient with the local Mach number. At the edge of the boundary layer, the scaling is near unity and the amount of background dissipation is sufficient to slightly degrade the solution. Without Mach-number scaling, background dissipation can degrade the entire solution.

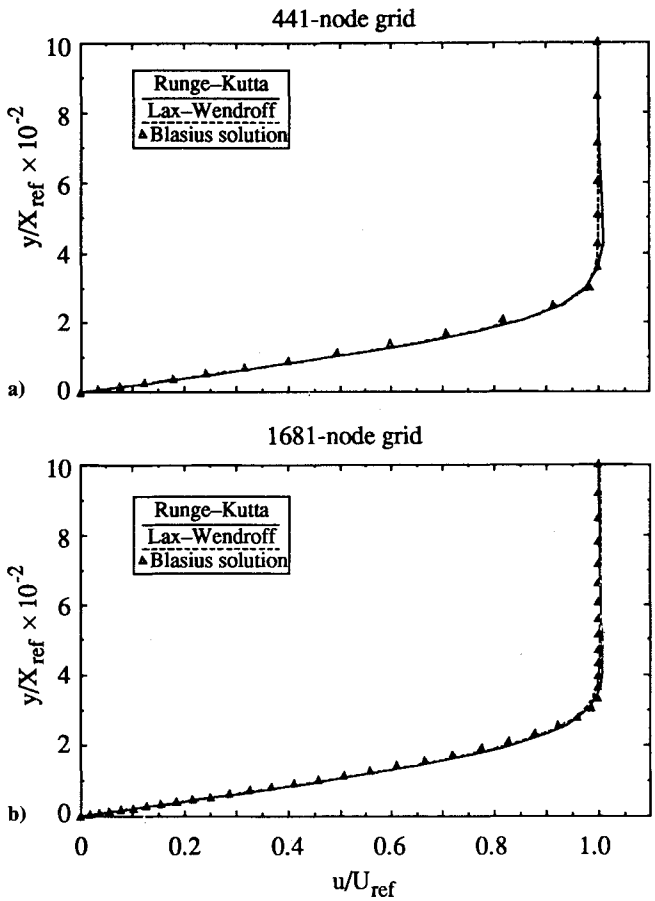

Fig. 7 Tangential velocity distributions for laminar flat plate flow at $M_\infty = 0.5$ and $Re_x = 5 \times 10^5$: a) for 441-node grid; b) for 1681-node grid.

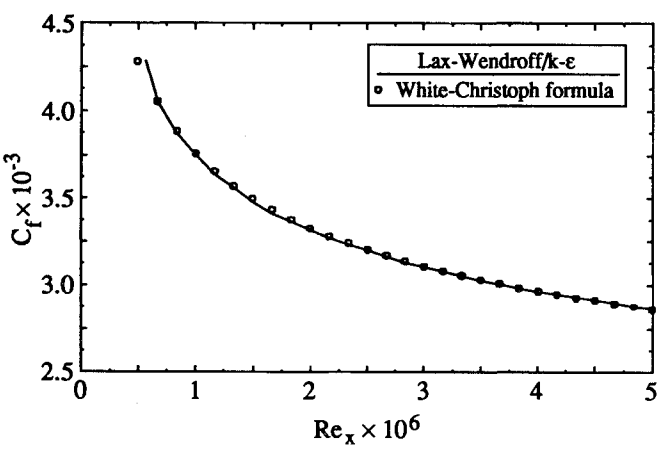

Fig. 8 C_f distributions for turbulent flat plate flow at $M_\infty = 0.5$.

Turbulent Flat Plate Flow

Turbulent flow over a flat plate was analyzed to verify the accuracy of the computed results in a turbulent flowfield. The 961-node grid is very similar to the grid illustrated in Fig. 5. For the nodes adjacent to the plate, y^+ is 2.5–3. The far-field Mach number is 0.5. Figure 8 compares the skin-friction coefficient distributions predicted using the Lax-Wendroff scheme with the White-Christoph formula.[32] Agreement between the computed results obtained with the high-Reynolds-number k-ε turbulence model and the White-Christoph formula is very good.

ONERA M6 Wing (Inviscid)

The inviscid flow over an ONERA M6 wing was computed to validate three-dimensional solutions. The case considered has a far-field Mach number of 0.84 and an angle of attack of 3.06 deg. The results for this case have been reported in Ref. 33. A summary of those results is included here for completeness. The 42,410-node grid used was generated using the advancing-front grid-generation scheme developed by Löhner.[31] The wing upper surface and symmetry plane boundary grids are illustrated in Fig. 9.

Pressure coefficient distributions on the wing surface for the computed results obtained using the Lax-Wendroff and Runge-Kutta schemes and for experimental data[34] are shown in Fig. 10 at three span locations. The computed results are in good agreement with the experimental data, with each other, and with other unstructured schemes.[33]

The Lax-Wendroff solution converged to three orders-of-magnitude reduction in the residuals within 1700 time steps and four orders-of-magnitude reduction within 2800 time steps. For the Runge-Kutta scheme, the solution was obtained by starting with the Lax-Wendroff solution and marching an additional 400 time steps.

ONERA M6 Wing (Viscous)

The final case considered is that for viscous flow over an ONERA M6 wing. This case was computed to validate solutions obtained in a three-dimensional viscous flowfield. The far-field Mach number is 0.84, the angle of attack is 3.06 deg, and the Reynolds number is 11.72×10^6. The grid used contained 203,383 nodes. For the nodes adjacent to the wing surface, y^+ is approximately 5. The wing upper surface and symmetry plane grids are illustrated in Fig. 11. Note that the

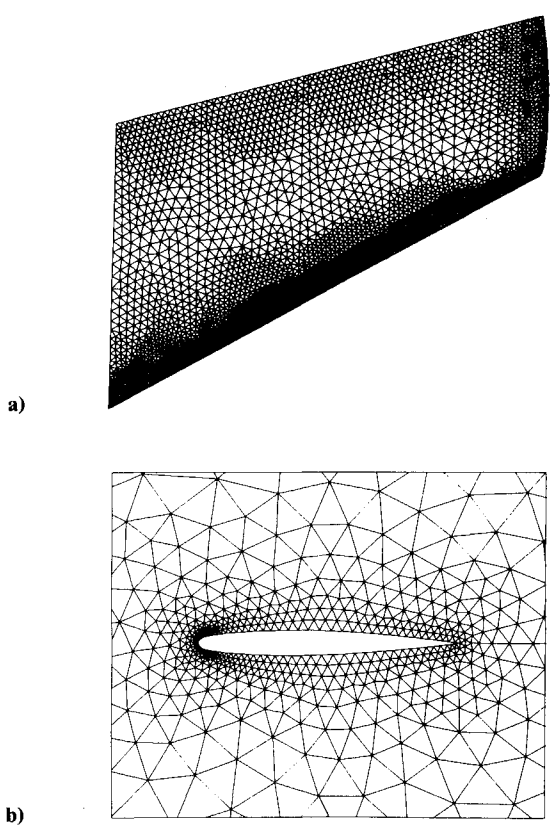

Fig. 9 Surface grids for ONERA M6 wing with 231,507 elements and 42,410 nodes: a) wing surface grid with 15,279 faces and 7680 nodes; b) symmetry plane grid with 1525 faces and 813 nodes.

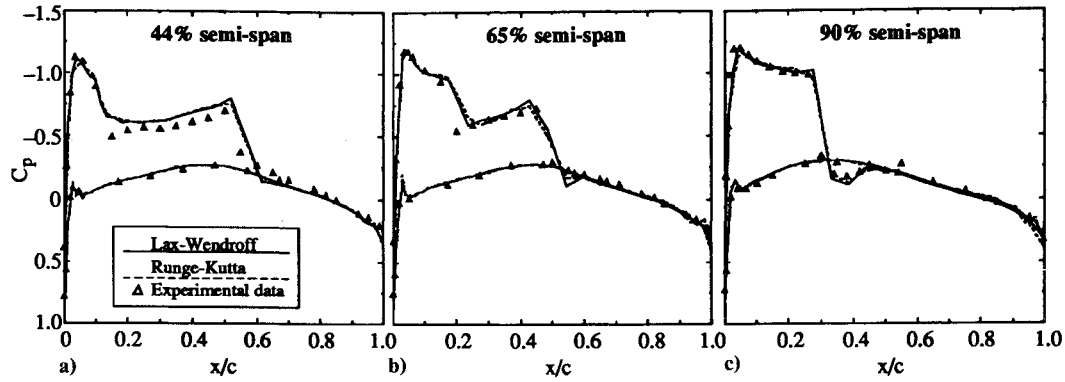

Fig. 10 C_p distributions for ONERA M6 wing at $M_\infty = 0.84$ and $\alpha = 3.06$ deg: a) 44% semi-span; b) 65% semi-span; c) 90% semi-span.

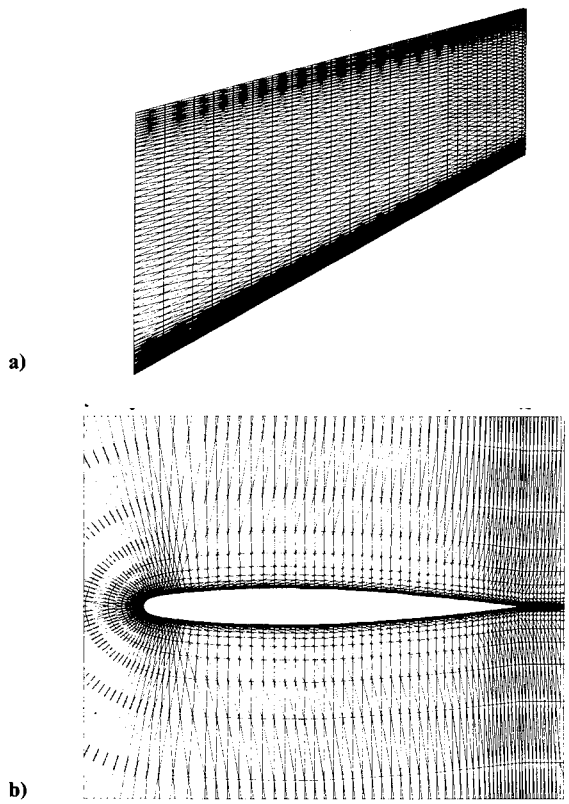

a)

b)

Fig. 11 Surface grids for ONERA M6 wing with 1,150,560 elements and 203,383 nodes: a) wing surface grid with 6,526 faces and 3,332 nodes; b) symmetry plane grid with 11,280 faces and 5,832 nodes.

wing surface grid has less than half the number of nodes for the previous case shown in Fig. 9.

Pressure coefficient distributions on the wing surface for the computed results obtained using the viscous Lax-Wendroff scheme with the low-Reynolds-number k-ε turbulence model are compared with experimental data[34] in Fig. 12 at three different span locations. The computed results are in good agreement with the experimental data and with the results obtained by Deese and Agarwal[35] using a finite volume Runge-Kutta scheme and a Baldwin-Lomax turbulence model. As expected, the computed locations of the wing upper surface shock waves are correctly upstream of those for the previous case shown in Fig. 10. However, the resolution of the shock waves is considerably less than for the previous case due to the coarser wing surface grid used in this case. The solution was obtained by marching 1000 time steps with inviscid flow, 1000 time steps with laminar flow, and 1500 time steps with turbulent flow.

Summary and Conclusions

A finite element Navier-Stokes code for unstructured grids has been developed. The code has been initially validated with computations of two- and three-dimensional inviscid and viscous flowfields. Through the use of an unstructured grid, the code is capable of computing flowfields about complex aerodynamic configurations and is ideally suited for grid adaption. The stated objective of developing a working Navier-Stokes code for investigation of viscous flowfield calculations using unstructured grid technology has been achieved. Future work will focus on improving efficiency and application to complex configurations and unsteady flowfields with moving bodies where the advantages of an unstructured grid can be fully realized.

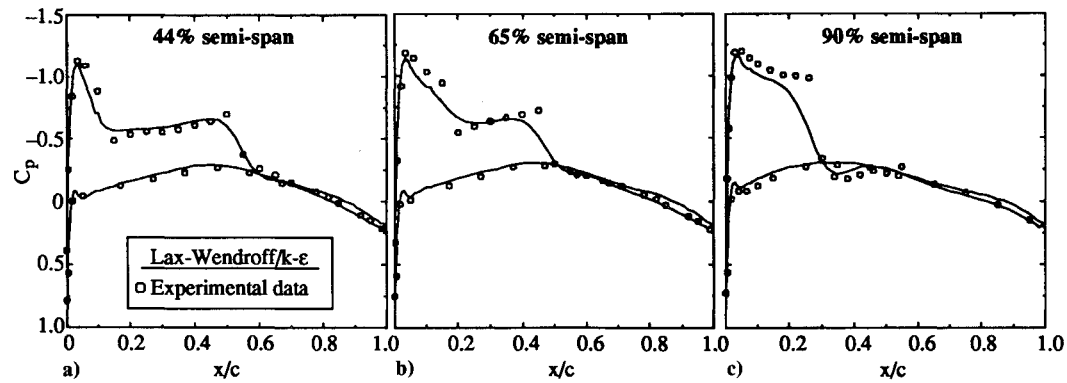

Fig. 12 C_p distributions for ONERA M6 wing at $M_\infty = 0.84$, $\alpha = 3.06$ deg, and $Re_c = 11.72 \times 10^6$: a) 44% semi-span; b) 65% semi-span; c) 90% semi-span.

Acknowledgment

This research was conducted under the McDonnell Douglas Independent Research and Development program.

References

[1]Jameson, A., Baker, T. J., and Weatherill, N. P., "Calculation of Inviscid Transonic Flow Over a Complete Aircraft," AIAA Paper 86-0103, 1986.

[2]Jameson, A., and Baker, T. J., "Improvements to the Aircraft Euler Method," AIAA Paper 87-0452, 1987.

[3]Löhner, R., and Baum, J. D., "Numerical Simulation of Shock Interaction with Complex Geometry Three-Dimensional Structures Using a New Adaptive H-Refinement Scheme on Unstructured Grids," AIAA Paper 90-0700, 1990.

[4]Parikh, P., Löhner, R., Gumbert, C., and Pirzadeh, S., "Numerical Solution on a PATHFINDER and Other Configurations Using Unstructured Grids and a Finite Element Solver," AIAA Paper 89-0362, 1989.

[5]Peraire, J., Peiro, J., Formaggia, L., Morgan, K., and Zienkiewicz, O. C., "Finite Element Euler Computations in Three Dimensions," AIAA Paper 88-0032, 1988.

[6]Stoufflet, B., Pariaux, J., Fezoui, F., and Dervieux, A., "Numerical Simulation of 3-D Hypersonic Euler Flows Around Space Vehicles Using Adapted Finite Element," AIAA Paper 87-0560, 1987.

[7]Mavriplis, D. J., "Euler and Navier-Stokes Computations for Two-Dimensional Geometries Using Unstructured Meshes," ICASE Rept. 90-3, Jan. 1990.

[8]Kallinderis, Y., and Baron, J. R., "Application of an Adaptive Algorithm to Single and Two-Element Airfoils in Turbulent Flow," AIAA Paper 90-0698, 1990.

[9]Rostand, P., "Algebraic Turbulence Models for the Computations of Two-Dimensional High-Speed Flows Using Unstructured Grids," *International Journal for Numerical Methods in Fluids*, Vol. 9, 1989, pp. 1121–1143.

[10]Holmes, D. G., and Connell, S., "Solution of the 2-D Navier-Stokes Equations on Unstructured Adaptive Grids," AIAA Paper 89-1932, 1989.

[11]Nakahashi, K., and Obayashi, S., "Viscous Flow Computations Using a Composite Grid," AIAA Paper 87-1128, 1987.

[12]Hassan, O., Morgan, K., and Peraire, J., "An Implicit Finite Element Method for High Speed Flows," AIAA Paper 90-0402, 1990.

[13]Bristeau, M., Mallet, M., Periaux, J., and Roge, G., "Development of Finite Element Methods for Compressible Navier-Stokes Flow Simulations in Aerospace Design," AIAA Paper 90-0403, 1990.

[14]Jones, W. P., and Launder, B. E., "The Calculation of Low-Reynolds-Number Phenomena with a Two-Equation Model of Turbulence," *International Journal of Heat & Mass Transfer*, Vol. 16, 1973, pp. 1119–1130.

[15]Launder, B. E., and Spalding, D. B., "The Numerical Computation of Turbulent Flows," *Computed Methods in Applied Mechanical Engineering*, Vol. 3, 1974, pp. 269–289.

[16]Marcum, D. L., and Agarwal, R. K., "A Three-Dimensional Finite Element Navier-Stokes Solver with k-ε Turbulence Model for Unstructured Grids," AIAA Paper 90-1652, 1990.

[17]Mavriplis, D. J., "Accurate Multigrid Solution of the Euler Equations on Unstructured and Adaptive Meshes," *AIAA Journal*, Vol. 28, No. 2, 1990, pp. 213–221.

[18]Löhner, R., Morgan, K., Peraire, J., Vahdati, M., "Finite Element Flux-Corrected Transport for the Euler and Navier-Stokes Equations," *International Journal for Numerical Methods in Fluids*, Vol. 7, 1987, pp. 1093–1109.

[19]Boris, J. P., and Book, D. L., "Flux Corrected Transport. I. SHASTA, A Fluid Transport Algorithm That Works," *Journal of Computational Physics*, Vol. 11, 1973, pp. 38–69.

[20]Zalesak, S. T., "Fully Multidimensional Flux-Corrected Transport Algorithms for Fluids," *Journal of Computational Physics*, Vol. 31, 1979, pp. 335–362.

[21]Rusanov, V. V., "The Characteristics of General Equations of Gas Dynamics," *Zhurnal Vychislitelnoi Mathematiki Mathematicheskoi Fiziki*, Vol. 3, 1963, pp. 508–527. Translated by K. N. Trirogoff, Literature Research Group, Aerospace Library Services, Aerospace Corp., Rept. LRG-65-T-38, 1965.

[22]Hoffman, J. D., "The Method of Characteristics Applied to Unsteady One-, Two-, and Three-Dimensional Flows," School of Mechanical Engineering, Purdue University, Rept. TR-80-07, 1980.

[23]Zucrow, M. J., and Hoffman, J. D., *Gas Dynamics*, Vols. 1 and 2, Wiley, New York, 1975.

[24]Marcum, D. L., and Hoffman, J. D., "Calculation of Three-Dimensional Subsonic/Transonic Inviscid Flowfields by the Unsteady Method of Characteristics," *AIAA Journal*, Vol. 23, No. 10, 1985, pp. 1497–1505.

[25]Marcum, D. L., and Hoffman, J. D., "Numerical Boundary Condition Procedures for Euler Solvers," *AIAA Journal*, Vol. 25, No. 8, 1987, pp. 1054–1062.

[26]Kentzer, C. P., "Discretization of Boundary Conditions on Moving Discontinuities," *Lecture Notes in Physics*, Vol. 8, Springer-Verlag, New York, 1970, pp. 108–113.

[27]Gielda, T. P., Deese, J. E., and Agarwal, R. K., "Three-Dimensional Delta/Thor Launch Vehicle Analysis Including Main Engine Plume Effects," AIAA Paper 91-3338, 1991.

[28]Bowyer, A., "Computing Dirichlet Tessellations," *Computer Journal*, Vol. 24, No. 2, 1981, pp. 162–166.

[29]Baker, T. J., "Three-Dimensional Mesh Generation by Triangulation of Arbitrary Point Sets," AIAA Paper 87-1124, 1987.

[30]Lo, S. H., "A New Mesh Generation Scheme for Arbitrary Planar Domains," *International Journal for Numerical Methods in Engineering*, Vol. 21, 1985, pp. 1403–1426.

[31]Löhner, R., and Parikh, P., "Generation of Three-Dimensional Unstructured Grids by the Advancing-Front Method," *International Journal for Numerical Methods in Fluids*, Vol. 8, 1988, pp. 1135–1149.

[32]White, F. M., and Christoph, G. H., "A Simple Theory for the Two-Dimensional Compressible Turbulent Boundary Layer," *Journal of Basic Engineering*, Vol. 94, 1972, pp. 636–642.

[33]Marcum, D. L., "Accuracy of a Finite Element Euler Solver for Unstructured Grids," NASA-Langley Workshop, "Accuracy of Unstructured Grid Techniques," Jan. 1990 (to be published).

[34]Schmitt, V., and Charpin, F., "Pressure Distributions on the ONERA-M6-Wing at Transonic Mach Numbers," AGARD-AR-138, 1979, Chap. B-1.

[35]Deese, J. E., and Agarwal, R. K., "Navier-Stokes Calculations of Transonic Viscous Flow About Wing/Body Configurations," *Journal of Aircraft*, Vol. 25, No. 12, 1988, pp. 1106–1112.